Low temperature relaxation of OH in the X 2 Π and A 2 Σ states in an argon free-jet

Michael M. Ahern and Mark A. Smith

Citation: The Journal of Chemical Physics **110**, 8555 (1999); doi: 10.1063/1.478763
View online: http://dx.doi.org/10.1063/1.478763
View Table of Contents: http://scitation.aip.org/content/aip/journal/jcp/110/17?ver=pdfcov
Published by the AIP Publishing

Articles you may be interested in

State-resolved distribution of OH X Π 2 products arising from electronic quenching of OH A Σ 2 + by N 2
J. Chem. Phys. **130**, 104307 (2009); 10.1063/1.3077027

Electronic quenching of OH A Σ + 2 radicals in single collision events with molecular hydrogen: Quantum state distribution of the OH X Π 2 products
J. Chem. Phys. **126**, 204316 (2007); 10.1063/1.2730505

Host-assisted intramolecular vibrational relaxation at low temperatures: OH in an argon cage
J. Chem. Phys. **125**, 024501 (2006); 10.1063/1.2212412

Rotationally inelastic collisions of OH (X 2 Π)+ Ar . II. The effect of molecular orientation
J. Chem. Phys. **113**, 637 (2000); 10.1063/1.481840

Rotationally inelastic collisions of OH (X 2 Π)+ Ar . I. State-to-state cross sections
J. Chem. Phys. **113**, 628 (2000); 10.1063/1.481839

This article is copyrighted as indicated in the article. Reuse of AIP content is subject to the terms at: http://scitation.aip.org/termsconditions. Downloaded to IP: 130.102.42.98 On: Sun, 23 Nov 2014 05:02:50

Low temperature relaxation of OH in the $X^2\Pi$ and $A^2\Sigma$ states in an argon free-jet

Michael M. Ahern and Mark A. Smith
Department of Chemistry, University of Arizona, Tucson, Arizona 85721

(Received 23 June 1998; accepted 12 January 1999)

Low temperature (translational temperatures below 10 K) relaxation of OH in the $X^2\Pi$ and $A^2\Sigma$ states has been studied in an argon free jet. We determine upper limits on $v=1$ relaxation in the $X^2\Pi$ manifold from laser induced fluorescence (LIF). We measure absolute relaxation rate coefficients for $v=2(N)$, $v=1(N)$, and $v=0(N)$ levels in the $A^2\Sigma$ state manifold. In addition, from comparison of the dispersed LIF we obtain state-to-state rate coefficients for $v=1$, $N=0$ and $N=1$ going to $v'=0,N'$ levels in the $A^2\Sigma$ manifold. Bimolecular rate coefficients are reported which are all much greater than similar measurements at room temperature. Rates for vibrational relaxation at these low temperatures are $5.7(\pm 0.7)\times 10^{-10}\,\mathrm{cm}^3/\mathrm{s}$ for $v(2-1)$ relaxation, $3.2(\pm 1)\times 10^{-10}\,\mathrm{cm}^3/\mathrm{s}$ for $v(1-0)$ relaxation, and we report rotational relaxation rates for $N=1$ and 2 of $v=0$, 1 and 2 excited states, all near the collision limited values. © *1999 American Institute of Physics.* [S0021-9606(99)00214-7]

I. INTRODUCTION

The OH radical is a key intermediate in a wide variety of chemical, atmospheric and astrophysical systems. The inelastic and chemical behavior of OH is important in such diverse environments as high temperature flames and low temperature planetary atmospheres. As a result, the temperature dependence of its inelastic and chemical behavior over wide ranges is of both applied and fundamental importance. We have recently reported some aspects of the chemical behavior of OH into the low temperature realm.[1–3] The OH radical has a large dipole moment, vibrational frequency and rotational constant similar to HCl and HF but as an open-shelled system, has very different chemical properties than those molecules. The inelastic collisional properties of ground state closed shell hydrides have been very well documented.[4] Open shell systems prove to be a greater challenge and thus the data is more limited. Owing to this reason, the fundamental nature of the OH radical and its natural importance, the low temperature rate behavior of the open shell OH system is particularly important to understand.

There have been numerous studies of OH relaxation at room temperature[5–14] but only a few using argon as the buffer gas. Argon, as with most rare gas atoms, is an inefficient relaxant at ambient temperatures. We have observed argon to be an effective rovibronic relaxant at the extremely low temperatures in free jets.[15] As a result, we chose to explore the relaxation efficiency of Ar with the polar OH system to determine the generality of inverse temperature dependence of inelastic rate processes in the extremes of low temperature. In the OH system, such behavior has been predicted by Copeland *et al.*[6]

Most of this study involves the measurement of energy transfer process occurring within the $A^2\Sigma$ state of the OH molecule. We have measured the low temperature (T_{trans}) below 10 K rate coefficients for specific OH rovibronic states,

$$\mathrm{OH}(A^2\Sigma, v_i, N_i) + \mathrm{Ar} \rightarrow \mathrm{OH}(A^2\Sigma, v_f, N_f) + \mathrm{Ar}, \qquad (1)$$

where v and N refer to the quantum numbers for vibration and pure rotational angular momentum, while the subscripts i and f refer to initial and final states, respectively. In addition, we are able to report upper bounds to the very slow vibrational relaxation rates observed for the $\mathrm{OH}^2\Pi_{3/2}$ state and some qualitative observations regarding efficient relaxation of rotation and fine structure label (total angular momentum) in the $\mathrm{OH}^2\Pi_J$ manifold.

II. EXPERIMENT

The free jet flow reactor used in this study has been extensively described in earlier reports.[16] To generate the OH/Ar flow, we employed a pulsed free jet consisting of 99.7% argon and 0.3% water. The water was triple deionized while the argon was UHP grade, both used without further purification. The mixture was prepared actively by combining argon and H_2O saturated argon flows from two independent flow controllers (Tylan model FC-280). The free jet nozzle was a Series 9 General Valve with a 0.4 mm diameter orifice, d, and was pulsed at 10 Hz (duty cycle of 125) with a backing pressure of 600–1200 Torr into a vacuum chamber with a pressure kept less than 10^{-4} Torr. After the water/argon mixture has left the nozzle, it continues to expand through an electrically grounded plate (thickness=0.3 mm) with a 1 mm hole at a downstream position of $z/d=4$, where z is the axial distance from the actual nozzle exit plane of diameter d. Another plate with a 4 mm hole which was floating at -600 V was positioned at $z/d=8$. Self-induced breakdown produced a transient discharge across the 2 plates generating the OH radicals. This arrangement leads to at least an open 40° aperture for the expanding gas emerging from the nozzle. Due to the nonspherical expansion of free jets in the initial few nozzle diameters, this effective aperture is most likely even larger. Since we sample only the angular aperture

 © 1999 American Institute of Physics

This article is copyrighted as indicated in the article. Reuse of AIP content is subject to the terms at: http://scitation.aip.org/termsconditions. Downloaded to IP: 130.102.42.98 On: Sun, 23 Nov 2014 05:02:50

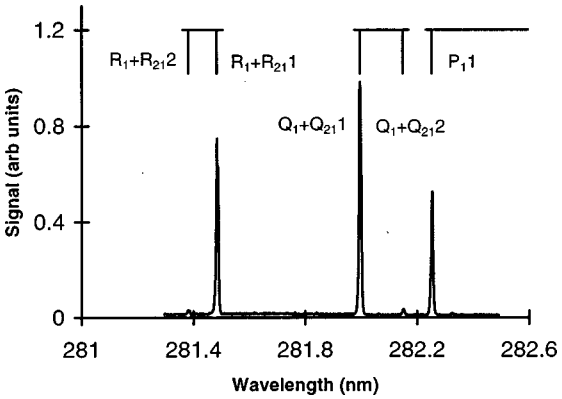

FIG. 1. Far field, terminally cooled laser induced fluorescence excitation spectrum of the OH $A-X$ (0–0) transition. The nozzle conditions were 900 Torr Ar. 0.3% water using a 0.4 mm diam nozzle. Excitation and fluorescence collection occurred at $z/d=20$.

corresponding to less than a central 17° of the flow, we feel that the discharge plates do not present a flow perturbation of significance to this study. This supposition is supported by the fact that the ratio of the mean free path to the aperture diameter (an effective Knudsen number in this case) at the position of each of the apertures is approximately 0.01. This effectively indicates a continuum flow regime near the apertures, where the aperture presence would not be expected to seriously effect the central flow streamlines at radial distances below 50% of the aperture diameters. In addition it indicates that the radicals generated in the plasma contained between the plates undergo many collisions in the subsequent expansion. This final argument is strongly supported by the extremely relaxed rotational and electronic state distributions of the OH radical, which is apparent in Fig. 1. Due to the much lower vibrational relaxation rates in the OH $X\,^2\Sigma$ state, to be discussed later, population in the OH $X(v=1)$ state is near 15%. However, it should be noted that the rotational/electronic distribution for OH$(v=0)$ and $(v=1)$ are identical.

The OH was laser excited using a Nd:YAG pumped dye laser to pump the $v=0$, 1, and 2 levels of the $A\,^2\Sigma$ state [for example, the $Q_1+Q_{21}(1)$ line wavelengths of 307.935 (0–0), 281.997 (1–0), and 288.314 (2–1) nm, respectively]. Fluorescence was measured perpendicular to the laser beam with an RCA 1P28 photomultiplier with a 0.5 m Czerny–Turner monochromator preceding it. The signal was fed to either a boxcar integrator (Stanford Research model 250) or a photon counter (Stanford Research model 460) depending on signal intensity. The two devices were calibrated for relative sensitivities using medium level signals. The outputs of the photon counter and the boxcar integrator were sent to a PC and signal averaged for 10–200 laser shots. A beam polarization scrambler was used before the monochromator to ensure that detection sensitivity enhancements due to polarization of different rotational branches were not present. The monochromator/photodetection system was calibrated for wavelength and response as a function of wavelength with a NIST-traceable mercury pen lamp (Oriel model 6035).[17]

Since the OH is made from discharge in a mixture of water and argon, it is found to produce a reasonable (15 $\pm 5\%$) population of OH $X\,^2\Pi_{3/2}$ $(v=1)$ population in the far field of the jet. This allows the ability to prepare and measure relaxation from the $v=2$ level of the $A\,^2\Sigma$ state, pumped here via the $A-X(2-1)$ transition, previously only accessible through the (2–0) band, which has a much less favorable transition probability.[18] It is important to point out, as can be seen from the spectrum in Fig. 1, that in the far flow field ($z>2$ cm or $z/d>50$, with $z/d=8$ being the position of the final discharge plate) the rotational state distributions of OH in either the $v=0$ or 1 level correspond to populations near 98% residing in the lowest rotational level, $N=1$. It is also interesting to note that observed population in the OH $^2\Pi_{1/2}$, which lies 139 cm^{-1} above the OH $^2\Pi_{3/2}$ $(v=0)$ level was populated at less than 1% of the ground state. By the point in which we could probe by LIF, beyond 0.8 cm, the vast majority of the nascent population in this higher fine structure state generated from the dissociation process appears to have been fully relaxed. Thus we have a kinetic situation where 98% of all the OH X state population resides in a single $^2\Pi_{3/2}$ $N=1$ lowest rotational level and we can specifically excite $v=0$ or $v=1$ levels for selective population transfer and kinetic analysis.

The relaxation rate coefficients are calculated by determining relative populations in different v,N states through detection of OH fluorescence of directly pumped A states as well as states not directly pumped but populated through collisional transfer. The first type of states will be termed ''initial states'' and the second kind of state will be termed ''transfer states.'' These transfer states have undergone either rotational or vibrational relaxation. The conversion of relative fluorescence intensities from either of these types of states to relative state populations is accomplished through the use of published line strength factors.[19,20] Comparison of transfer state populations to initial state populations as a function of laser probe position from the nozzle is used to determine rates of relaxation for OH in the A state (see Appendix). Thus, as one probes farther down the jet axis, the number of collisions occurring during the average fluorescent lifetime decreases as $1/z^2$. Since the fluorescence lifetime is much less than the transit time of the jet across 1 mm, the sample can be considered spatially fixed during this fluorescence clock time. In this way the fluorescence lifetime serves as the reaction clock for a sample at a known density and temperature. Comparisons of total fluorescence intensity as a function of distance are used to determine rates for transfer processes in the OH $X\,^2\Pi$ and $A\,^2\Sigma$ states.

III. RESULTS

Conversion from signal intensity to relative state populations is needed to measure the relaxation rate coefficients. The transition probability or Einstein coefficient for emission, $A_{v''N''}^{v'N'}$ in a given $(v'N'-v''N'')$ band, may be written

$$A_{v''N''}^{v'N'}=\frac{64\pi^4}{3hc^3}p_{v''N''}^{v'N'}S_{N'N''}\frac{(\nu_{v''N''}^{v'N'})^3}{2N'+2}, \tag{2}$$

where $p_{v''N''}^{v'N'}$ is the probability for the transition between the two vibration-rotation levels, $S_{N'N''}$ is the rotational line-

This article is copyrighted as indicated in the article. Reuse of AIP content is subject to the terms at: http://scitation.aip.org/termsconditions. Downloaded to IP: 130.102.42.98 On: Sun, 23 Nov 2014 05:02:50

strength, and $\nu_{v''N''}^{v'N'}$ is the average frequency of the transition. The quantum number N (labeled K by Dieke and Crosswhite[21]) is defined as total angular momentum minus spin and is always an integer, thus $N=J-\frac{1}{2}$ for OH. This notation is strictly only applicable in Hund's Case B coupling but is used for both the $X\,^2\Pi$ (case A) and $A\,^2\Sigma$ (case B) states of OH, consistant with notation used by Dieke and Crosswhite and almost all subsequent OH relaxation studies. The intensity of a band, or power radiated from 1 cm^3 of the gas containing $n_{v'}$ molecules in the v' (upper) vibrational level, is

$$I_{v''N''}^{v'N'}=n_{v'N'}h\nu_{v''N''}^{v'N'}A_{v''N''}^{v'N'} \tag{3}$$

and has units of erg $cm^{-3}\,s^{-1}$. In this study, selected A factors were measured and compared to the detailed study and literature survey of Crosley and Lengel.[20]

In the absence of self-absorption, the ratio of different fluorescence transition intensities from transitions with the same upper vibrational level should be a constant. In our study, pumping $N=1$ and collecting all fluorescence, we measured the A_1^2/A_2^2 ratio via the following relationship

$$\frac{A_1^2}{A_2^2}=\frac{I_1^2\nu_2}{I_2^2\nu_1}, \tag{4}$$

where $n_{N'v'}$ from the above equation drops out if the upper vibrational level is the same for both transitions. We found the A_1^1/A_0^1 and A_1^2/A_2^2 ratios and compared them to literature values. The ratios, within experimental error are equivalent to previous measurements.[20] For calculating rate coefficients we use the rotational transition probabilities of Chidsey and Crosley[19] and vibrational Einstein A factors of Crosley and Lengel[20] without any corrections.

A. Rotational relaxation

The rotational relaxation rate coefficients for the OH $A\,^2\Sigma$ $v=0$, 1, and 2 states were measured. There was specific interest in the question of whether the predissociative nature of the $v=2$ state would affect the rate of relaxation. The $v=2$ state has a much shorter lifetime than the $v=1$ state due to predissociation and lifetime comparisons are shown in Fig. 2. Our lifetime measurements are in agreement with those of Brzozowski *et al.*,[22] showing that there was not significant electronic quenching of OH in the $A\,^2\Sigma$ state by any of the species in the free jet meaning that during the fluorescence lifetime the OH remains in a single collision dominated regime.

The rotational relaxation is as follows:

$$\mathrm{OH}(v,N)+\mathrm{Ar}\rightarrow\mathrm{OH}(v,N-1 \text{ or } N-2)+\mathrm{Ar}. \tag{5}$$

The OH in state (v,N) collides with an argon atom and relaxes to a lower rotational level within the same vibrational level. The fluorescence from both the OH (v,N), and the OH $(v,N\text{-}1$ or $N-2)$ in the A state can be detected with the monochromator.

The $X-A$ pump energy and wavelength are kept constant, leading to constant preparation of an initially selected OH $A\,^2\Sigma(v,N)$ state, while the monochromator is scanned. The upper state fine structure emission in our experiment is

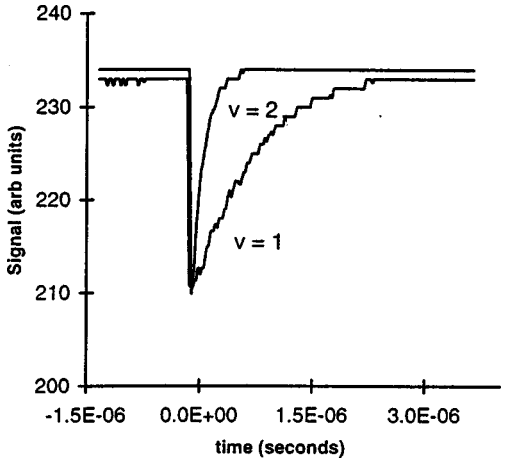

FIG. 2. Time dependence of the total fluorescence decay curves for the OH $X-A(v)$ transitions. The fluorescence lifetime of the OH $A\,^2\Sigma$ $(v=2)$ state is significantly reduced relative to the low N, $v=1$ or 0 levels owing to predissociation induced by mixing with the near lying crossing of the dissociative OH $^4\Sigma$ state (Ref. 16).

not resolvable. For example, $R_1 1$ and $R_{21}1$ are unresolved under our conditions. The peaks were assigned and labeled with the notation of Dieke and Crosswhite.[21] (A very good program by Luque and Crosley[23] tabulates line positions, A and B factors and makes spectral simulations.) When the $R_1 1(0-0)+R_{21}1(0-0)$ line is pumped, (under high power conditions, both lines are pumped within the resolution of the laser), there are many lines that can be seen when dispersing the emission without relaxation, namely the $R_1 1+R_{21}1$, $R_2 1$, $Q_1 2+Q_{21}2$, $Q_2 2+Q_{12}2$, $P_1 3$, $P_{12}3+P_2 3$, and $O_{12}4$ lines. The convention used is such that lines with only one subscript have the upper and lower fine state number equal. For example, $R_2 1$ means that the lower and upper fine structure state is the one labeled 2 and the 1 indicates the value of N. Sometimes these two fine states are referred to as F_1 and F_2. For a label with 2 subscripts, the first one is the level in the upper state, the A state, and the second is the lower state, the X state. The upper case number remains N for the lower, X state.

Initially, some rotational level, N, of the $A\,^2\Sigma$ state is populated by the laser. At close distances from the nozzle, the higher density leads to greater relaxation before fluorescence, yielding newly populated relaxed states, which lead to new lines in the emission spectrum. The $P_{21}1$ and $P_1 2+P_{21}2$ lines shown in Fig. 3(a) are larger than the $P_1 3+P_{21}3$ line which originates from the initially prepared state at $z=0.4$ cm. When $z=1.2$ cm, as in Fig. 3(b), the number of collisions is reduced due to the decreased number density and so the populations of molecules that underwent relaxation are decreased with respect to the directly populated states.

Multiple scans, similar to Fig. 3, are made at varying distances from the nozzle. Derivation of a rotational rate coefficient for such a data set is outlined in the Appendix. A rate coefficient is determined from the integrated rate relationship

This article is copyrighted as indicated in the article. Reuse of AIP content is subject to the terms at: http://scitation.aip.org/termsconditions. Downloaded to IP: 130.102.42.98 On: Sun, 23 Nov 2014 05:02:50

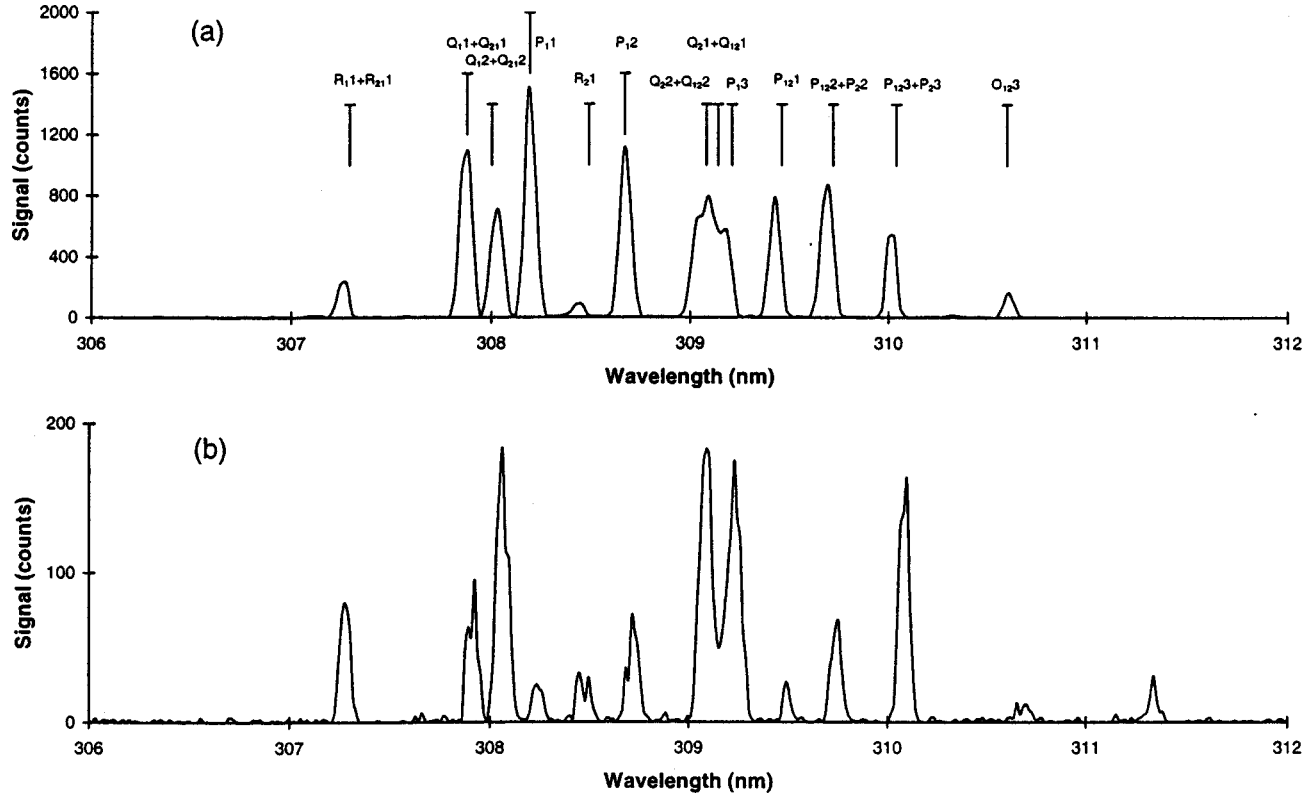

FIG. 3. Example of the axial position dependence of rotational relaxation within the OH A $^2\Sigma$ ($v=0$) rotational manifold during the initial state radiative lifetime. The initial state corresponds to OH $A\,^2\Sigma$ ($v=0$, $N=2$). When excitation occurs close to the nozzle, as in (a) at 0.4 cm, emission from OH $A\,^2\Sigma$ ($v=0$, $N=0$, 1, and 2) is observed due to pure rotation collisional relaxation in the reasonably dense free jet. At farther axial distances in the jet, as in (b) at 1.2 cm, the emission begins to show less relaxation and the emission predominates from the initially prepared state.

$$\frac{I_{\mathrm{ref}}}{I_{N'}}=\frac{k_{fi}z^2}{k_{N-N'}M_0z_0^2}+\frac{k_Q'}{k_{N-N'}}. \tag{6}$$

Here $I_{N'}$ is the relative number density of the state to which population has been transferred while I_{ref} is the total relative number density for molecules initially excited to the OH $A\,^2\Sigma(v,N)$ state. $I_{N'}$ is obtained from the integrated fluorescence intensity of all OH lines originating from the OH $A\,^2\Sigma(v,N')$ transfer state, while I_{ref} derives from the sum of the intensity of all lines corrected for rotational line strength factors. The value, k_{fi}, corresponds to the fluorescence rate from the initially pumped state, determining the clock by which relaxation must compete against. The quantity, $(M_0z_0^2/z^2)$, where M_0 is the stagnation density of the relaxant gas and z_0 is a distance scale related to the nozzle orifice diameter, represents the local density of the relaxant M at axial position z in the flow.[16] Since the quantities, k_{fi}, M_0, and z_0 are all well known, the slope from a plot of $I_{\mathrm{ref}}/I_{N'}$ vs z^2 provides a direct measure of the absolute state-to-state rotational transfer rate coefficient, $k_{N-N'}$. In the case where more than one relaxation channel is present, as in OH $A\,^2\Sigma$ ($v=0$, $N=2$), the total relaxed population is used and the total relaxation rate is obtained. Using the relative product fluorescence line intensities extrapolated to the limit of no relaxation (i.e., to single collision conditions) provides the nascent branching ratios for product states allowing the total rate to be deconvoluted into the state specific rates. An example of such a plot of $I_{\mathrm{ref}}/I_{N'}$ is shown for the total OH $A\,^2\Sigma$ ($v=0$, $N=2$) state in Fig. 4. The total and state-to-state rotational relaxation rate coefficients are listed in Table I. From the intercepts of the integrated rate plots (Fig. 4), we can obtain values of k_Q, the pure electronic quenching rate coefficient. This quenching rate is found to be very slow. The observed values of k_Q are always less than 20% of all other collisional processes being measured.

As can be seen, all rotational transfer rate coefficients are quite large at the very low temperatures present in the

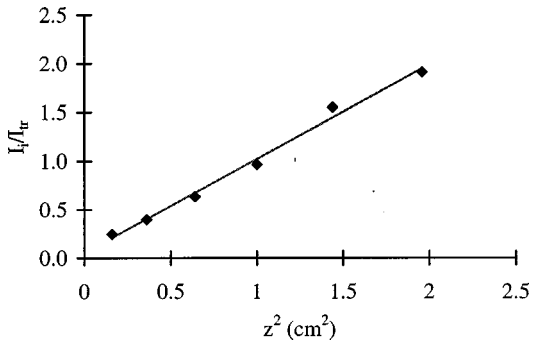

FIG. 4. A fit of fluorescence intensity to the integrated rate law, Eq. (6) for the pumping of the OH $A\,^2\Sigma$ ($v=0$, $N=2$) state. The slope of the line yields a total rotational relaxation rate coefficient of 1.80×10^{-10} cm^3 s^{-1} for the 10 K collisional conditions within the free jet. From the relative rotational line strengths observed in the dispersed spectrum, the state-to-state or detailed rotational relaxation rate coefficients reported in Table I are obtained.

This article is copyrighted as indicated in the article. Reuse of AIP content is subject to the terms at: http://scitation.aip.org/termsconditions. Downloaded to IP: 130.102.42.98 On: Sun, 23 Nov 2014 05:02:50

TABLE I. Relaxation rate coefficients for OH $A\,^2\Sigma$ in collisions with Ar (in units of $10^{-11}\,cm^3\,s^{-1}$).

Rotational relaxation from:	$T=300$ K	$T<10$ K (this work)
$v=2$, $N=2$		20 ± 4
$v=2$, $N=1$		13 ± 4.5
$v=1$, $N=2$		11 ± 2
$v=1$, $N=1$		6.7 ± 1
$v=0$, $N=2$		$k_{tot}=18\pm2$
		$k_{2-1}=12\pm1$
		$k_{2-0}=6.0\pm1$
$v=0$, $N=1$		6.6 ± 1
Vibrational relaxation from:		
$v=2$		5.7 ± 2.6
$v=1$	0.41 ± 0.03[a]	3.2 ± 0.8

[a]L. R. Williams and D. R. Crosley, J. Chem. Phys. **104**, 6507 (1996).

free jet. It is interesting to note that the rotational relaxation rates in the free jet, for both $\Delta N=1$ and 2 are significantly greater than those values observed for higher N levels at 300 K by Jorg *et al.*[31]

B. Vibrational relaxation

The vibrational relaxation rates we report are for the following process:

$$\mathrm{OH}\ A\,^2\Sigma(v,N)+\mathrm{Ar}\rightarrow\mathrm{OH}\ A\,^2\Sigma(v-1,N')+\mathrm{Ar}. \quad (7)$$

We report vibrational relaxation from the $v=2$ to $v=1$ state and the $v=1$ to $v=0$ state. Relaxation of $v=2$ to $v=0$ could not be detected within our signal to noise. Less than 5% of the $v=2$ population relaxing undergoes a $\Delta v=-2$ transition. Comparison of product branching into particular N' levels allows, in principle, conversion of the total vibrational relaxation rate coefficient (summed over all N') to be converted to v,N to v',N' state-to-state coefficients. Unfortunately these product branching ratios required to generally accomplish this could not be easily obtained under single collision conditions. As a result we must settle for partially relaxed product distributions. These are reported in Fig. 6 while the total rates, not affected by this are given in Table I. We have also been able to determine upper limits to the very slow total relaxation rate of the OH $X\,^2\Pi_{3/2}\,(v=1)$ state also shown in Table I.

The first vibrational relaxation rate that will be discussed is the relaxation of $v=1$ in the $X\,^2\Pi$ state. This was measured via the methods previously described by this laboratory for the determination of rate coefficients for reactions within free jet flows.[16] The method uses the loss of reactant density as a function of flow distance to calculate a vibrational relaxation rate coefficient. In our experiment we observe no relaxation of the $v=1$ $X\,^2\Pi_{3/2}$ state and are able only to calculate an upper bound for relaxation of the $v=1$ $X\,^2\Pi$ state of $k<5\times10^{-13}\,cm^3/s$. Due to intrinsic limitations owing to the low jet densities, this upper bound for a rate coefficient is more generous than that of room temperature experiments.[7,8] As will be shown, however, it is at least three orders of magnitude slower than vibrational relaxation in the $A\,^2\Sigma$ state.

The determination of vibrational relaxation rate coefficients for the $A\,^2\Sigma$ state are similar to the method employed for rotational relaxation. One difference in the data analysis involves the need to measure the relative populations of the $v''=0$ and $v''=1$ levels in the $X\,^2\Pi_{3/2}$ state. This was accomplished before rates could be calculated. To measure relative populations, the $P_1 1(0-0)$ and $P_1 1(1-1)$ bands were excited at varying laser intensities with the monochromator set to a resolution of 8 nm in order to collect all emission of an individual vibrational transition. The $P_1 1(0-0)$ excitation was followed by collection of all rotational branches of (0–0) emission. Similarly, when the $P_1 1(1-1)$ band was excited, all rotational branches of (1–1) emission were collected.

Data were taken at a wide variety of laser powers owing to difficulty of obtaining OH spectra under either completely saturated or completely unsaturated conditions. At low powers the relationship between signal intensity and number of molecules in a particular state is given by[23]

$$I_{v''N''}\propto n_{v''N''}\times B^{v''N''}_{v'N'}\times\tau\times\sum A^{v'N'}_{v''N''}\times(1-e^{-(t/\tau)}), \quad (8)$$

where $I_{v''N''}$ is the fluorescence intensity of the emission collected when exciting molecules from the $v''N''$ ground state, $n_{v''N''}$ is the number density of molecules in the $v''N''$ ground state, $B^{v''N''}_{v'N'}$ is the Einstein B-coefficient for absorption from the $v''N''$ level. Here $\Sigma A^{v''N''}_{v'N'}$ represents the sum of all Einstein A coefficients for spontaneous emission from the $v'N'$ upper state, τ is the lifetime of the $v'N'$ excited state, and t is the time following which the fluorescence was collected after the laser excitation. In our case, we collected emission from the LIF for times much longer than the lifetime of the state so the last term in the above equation goes to unity.

At high powers the relationship between initial state number density and emission intensity simplifies to

$$I_{v''N''}\propto n_{v''N''}\times\frac{\Sigma A^{v'N'}_{v''N'}}{\tau}. \quad (9)$$

We compared our relative populations of ground state $v'=0$ and $v=1$ in the limits of low and high laser power using the above relationships. We determined an $\mathrm{OH}\,X\,^2\Pi_{3/2}(v=0)/\mathrm{OH}\,X\,^2\Pi_{3/2}(v=1)$ population ratio of 7.0 ± 0.3 independent of the power limit and constant under all of the conditions employed in this study. This quantity can now be used to derive an expression relating dispersed LIF emission intensities from the pumping of either OH $X\,^2\Pi(v)$ state to vibrational relaxation rate coefficients. A full derivation of this relationship is provided in the Appendix and only the result is given here

$$\frac{I_{\mathrm{ref}}}{I_{v'}}=\left(\frac{\mathrm{tr}'_{v'}(z,t=0)}{i_v(z,t=0)}\times\frac{(k_{pd}+k_{fi})}{M_0 z_0 k_{\mathrm{rel}}}\right)z^2+\left(\frac{k_{\mathrm{rel}}+k_Q}{k_{\mathrm{rel}}}\times\frac{\mathrm{tr}'_{v'}(z,t=0)}{i_v(z,t=0)}\right). \quad (10)$$

The ratio, $tr'_{v'}(z,t=0)/i_v(z,t=0)$ is determined by consideration of the relative Einstein B coefficients for the pumped

This article is copyrighted as indicated in the article. Reuse of AIP content is subject to the terms at: http://scitation.aip.org/termsconditions. Downloaded to IP: 130.102.42.98 On: Sun, 23 Nov 2014 05:02:50

transitions preparing $tr'_{v'}$ and i_v and the original state populations (if different) for the OH $X\,^2\Pi(v)$ levels used. Since the quantities, k_{pd}, k_{fi}, M_0, z_0, $(tr'_{v'}(z,t=0)/i_v(z,t=0))$ are known, k_{rel} can be determined from a plot of $I_{\mathrm{ref}}/I_{v'}$ vs z^2. It is important to note that the determination of all of the rate coefficients in this study is independent of which saturation regime one is in when preparing the OH A state. That is due to the fact that all analyses are independent of the absolute population in the single initially prepared $A\,^2\Sigma(v,N)$ level.

The vibrational relaxation rate coefficients for the $A\,^2\Sigma$ $v=2$ and $v=1$ states are shown in Table I. Note that all $A\,^2\Sigma$ vibrational relaxation rates are of the order of magnitude of both the rotational rates and the total collision rates. The vibrational rate coefficients appear to be independent of the rotational level pumped in this study. Adding one quanta of rotational energy did not affect the vibrational relaxation rates for either state within our error limits.

C. Rotational partitioning in vibrational relaxation

By employing the monochromator at its maximum operable resolution, the vibrationally relaxed emission can be resolved into its rotational components. One example of this dispersed emission is shown in Fig. 5. For $v(1-0)$ relaxation of the A state, the rotational distribution was measured from the intensities of the $v=0$ emission in the limit of early relaxation time. The large lines at longer wavelength are due to the (1–1) band of the $A-X$ transition, including the effects of $N=1$ to $N'=0$ relaxation within the $v=1$ manifold. The smaller lines at shorter wavelength are due to the vibrational relaxation of the $v=1A$ state producing $A(0-0)$ emission from a wide range of final N' levels in the $v=0$ manifold. The intensity of the (0–0) lines are enhanced by a greater Einstein A coefficient, $A_0^0/A_1^1=1.7$.[20]

The distribution of population with N' quanta of rotational energy is shown in Figs. 6(a) and 6(b) for relaxation of OH $A\,^2\Sigma$ $(v=1, N=1)$ and OH $A\,^2\Sigma$ $(v=1, N=0)$, respectively. The conditions of the relaxation are such that on the average, only 10% undergo a collision. The error on the populations in Fig. 6 is approximately 20% with an absolute error of 1.5% for the $N=12$ and 13 levels. The distributions in Fig. 6 were produced iteratively using the Lifbase software of Luque and Crosley.[23]

Relaxation spectra taken at different distances from the nozzle showed no population differences, which was a check that the OH molecules were truly in the low collision limit. If there had been many relaxing collisions per molecule, one would expect spectra taken at higher density (closer to the nozzle), to have colder distributions. It is interesting to note that the rotational distribution of products having undergone one quanta of vibrational relaxation in the $A\,^2\Sigma$ state is neither a Boltzmann distribution nor the cold distribution produced by a free jet. In addition, the two graphs look very similar showing that the one extra quanta of rotation makes little difference in the partitioning of the vibrational relaxation. The population appears to be strongly distributed among states from $N=1$ to 10, tapering off when the rotational energy of the product approaches the vibrational energy being lost in the reactant. The $N'=8,9,10$ levels seem to be the most favored products. The $v'=0$, $N'=12$ level of the $A\,^2\Sigma$ state at 35 038 cm^{-1} is the closest exothermically accessible state to the $v=1$, $N=0$ state at 35 429 cm^{-1}. The observed population of 2% in $v=0$, $N=13$ in the $v=1$, $N=0$ relaxation is consistent, within the errors, of a mean translational temperature below 10 K. The $v=1$, $N=2$ state at 35 461 cm^{-1} is high enough that the relaxation to $v'=0$, $N'=13$ at 35 459 cm^{-1} is exothermic. The energies of the states were taken from the work of Coxon.[24]

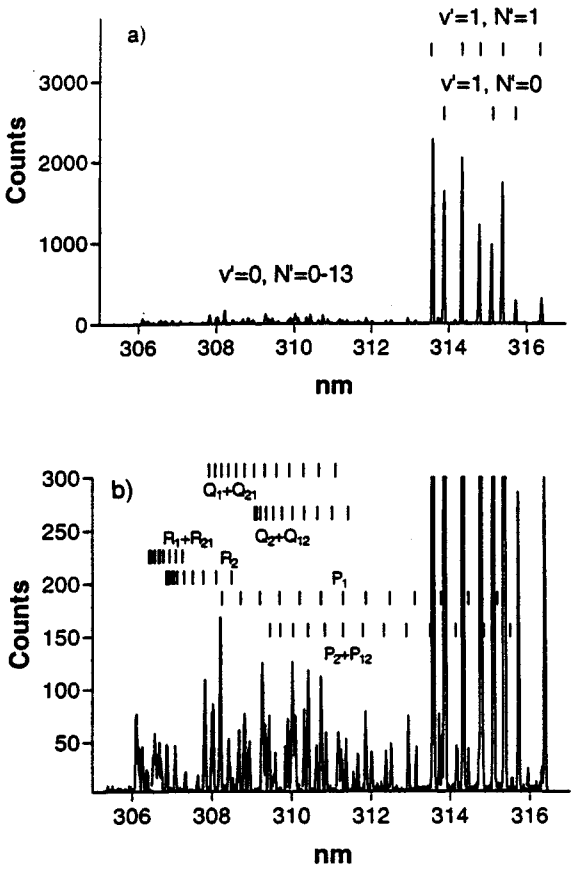

FIG. 5. Dispersed fluorescence spectrum of the OH $X-A$ transition following excitation of the $Q_1 1$ (1–0) line at a position of $z=1.0$ cm in an Ar free jet of stagnation pressure 900 Torr and $d=0.4$ cm. (a) Low amplification spectrum highlighting rotational relaxation from $N=1$ to $N'=0$ within the OH $A\,^2\Sigma$ $(v=1)$ manifold. (b) Expanded scale of the same spectrum highlighting emission from OH $A\,^2\Sigma$ $(v=0, N'=0-12)$ induced by vibrational relaxation caused by OH $A\,^2\Sigma$ $(v=1, N=1)$–Ar collisions.

The relaxation of the $A\,^2\Sigma$ $(v=1, N=1)$ originates from both of the fine states populated by the excitation laser. Their intensity distribution determined by dispersed fluorescence shows no propensity to go to the $^2\Pi_{3/2}$ vs the $^2\Pi_{1/2}$ state. A more interesting case is when the excited state is the $A\,^2\Sigma$ $(v=1, N=0)$ state which has only one fine state level, the F_1. The vibrational relaxation of this level still shows no propensity to go to one or the other lower fine state (F_1 vs F_2) showing that the electronic states are completely and randomly scrambled during a vibrationally inelastic collision.

This article is copyrighted as indicated in the article. Reuse of AIP content is subject to the terms at: http://scitation.aip.org/termsconditions. Downloaded to IP: 130.102.42.98 On: Sun, 23 Nov 2014 05:02:50

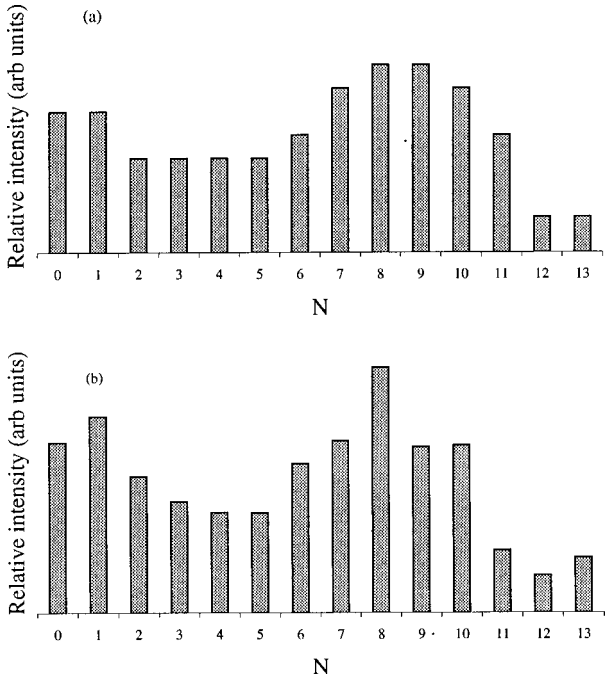

FIG. 6. The rotational dependence of vibrational relaxation showing nascent distribution of population in the $v=0$ level of A state after excitation into the $v=1$ level of the OH $A\,^2\Sigma$ state. (a) Distribution when exciting the $N=1$, $v=1$ level. (b) Distribution when exciting the $N=0$, $v=1$ level.

A comparison of rotational partitioning at room temperature can be made using the study of Lengel and Crosley.[11] The authors were not able to measure relaxation of OH with argon but were able to use hydrogen and nitrogen as buffer gases. Their high-resolution spectra of OH having undergone vibrational relaxation to multiple N states looks qualitatively similar to ours for Ar (Fig. 5). They fit their rotational partitioning to a Boltzmann relationship, which gave a rotational temperature of 670 K for hydrogen and 900 K for nitrogen. There is no *de facto* reason that the distribution of rotational states should be a Boltzmann distribution, but if we fit ours to such a relationship for comparison we obtain temperatures near 1200 K for relaxation of $v=1$, $N=0$ and $N=1$, respectively. It appears that we observe significantly greater rotational excitation of our product distributions in this low temperature OH–Ar relaxation. Also, our rotational distributions display greater deviations from a thermal relationship compared with those of Lengel and Crosley.[11]

IV. DISCUSSION AND CONCLUSIONS

We have measured rotation-vibration relaxation rate coefficients of OH in both the A and X states at the low translational temperatures within the core of an Ar free jet (T_{trans} below 10 K). From the observed rotational temperatures in the OH X state, it appears that rotational relaxation in this manifold is extremely fast, as would be expected from consideration of rotational cooling in a wide variety of molecules in free jets.[25] In addition, the absence of any observable OH $X\,^2\Pi_{1/2}$ $(v=0)$ indicates that this low energy excited state relaxes rapidly under the jet conditions. A similar result for the fine structure excited state of NO (Ref. 15) is well known. It is interesting to note that fine structure relaxation of the very strong collisions of $Xe^+\,^2P_{1/2}$ with a variety of rare gases, including Ar, showed no evidence of relaxation in the 1 K limit.[26] Also in contrast with NO, electronic quenching remains slow for OH $A\,^2\Sigma$ in the near zero Kelvin limit, as observed in this study.

Vibrational relaxation of OH $X\,^2\Pi_{3/2}$ $(v=1)$ by Ar was found to remain extremely slow at the free jet temperatures. This is consistent with the known poor efficiency of Ar as a vibrational relaxant at higher temperatures, but is in contrast to studies of NO^+ $(v=1)$ relaxation by Ar near 1 K.[15] In this latter study, Ar was found to relax NO^+ $(v=1)$ with near single collision efficiency. It would appear that the weaker long-range attraction of the dipole-atom interaction potential in OH $X\,^2\Pi-$Ar collisions as compared to the strong ion-induced dipole NO^+-Ar interactions must play a role here. Long-lived complex formation has been used to explain the strong inverse temperature dependence of many relaxation processes in the low temperature limit.[27,28] In the case of OH $X\,^2\Pi$ $(v=1)$, it would appear that the complex lifetimes remain sufficiently short that vibrational predissociation of the complex remains poorly competitive with simple adiabatic back-dissociation along the incoming potential surface.

The case of low temperature OH $A\,^2\Sigma$ rotation/vibration relaxation appears quite different from that in the OH $X\,^2\Pi$ manifold. In OH $A\,^2\Sigma$ (v,N) levels, vibrational relaxation by Ar appears to be strongly competitive with rotation, both occurring near the collision limit. The collision rate coefficient can be well approximated using a capture model for complex formation. Employing a two term long range interaction potential including both dipole-induced dipole and simple dispersion terms, one can derive a simple expression for the capture rate

$$k_{\text{capture}}=6\pi^{1/2}\Gamma(5/3)\left(\frac{\epsilon\alpha^6}{2\mu}\right)^{1/3}\left(\frac{2k_bT}{\mu}\right)^{1/6}, \tag{11}$$

where μ is the collision pair reduced mass, $\Gamma(x)$ is the gamma function, and the effective Lennard-Jones parameters, $\epsilon\sigma^6$, can be represented by the expression

$$\epsilon\sigma^6=\frac{\mu_{\text{D}}^2\alpha_{\text{Ar}}}{4}+\frac{3\alpha_{\text{OH}}\alpha_{\text{Ar}}}{16}\left(\frac{\text{IP}_{\text{OH}(A)}\text{IP}_{\text{Ar}}}{\text{IP}_{\text{OH}(A)}+\text{IP}_{\text{Ar}}}\right), \tag{12}$$

where μ_1, α_1, and IP_1 represent dipole moment, polarizability, and ionization potential of the ith component.[29] Using a calculated value (DFT) for the polarizability of the OH A state of $6.9\times10^{-31}\,\text{m}^3$ and experimental values for all other quantities, we obtain an OH $A\,^2\Sigma-$Ar collision capture rate coefficient value between 6 and $9\times10^{-11}\,\text{cm}^3/\text{s}$ in the temperature window between 1 and 10 K, respectively. This range of values compare very favorably with the total relaxation rate coefficients observed in the jet for the OH $A\,^2\Sigma$ state in either the $v=0$ or $v=1$ state.

It appears that energy transfer in the OH $A\,^2\Sigma$ state by Ar occurs for every collision. In the case of OH $A\,^2\Sigma$ $(v=1, N=1)$, pure rotational transfer proceeds roughly twice as fast as vibration, whereas in OH $A\,^2\Sigma$ $(v=2, N=1)$ vibrational energy transfer appears to display an efficiency twice that of simple rotational relaxation. The pure rotational relaxation processes studied appear to display only modest

This article is copyrighted as indicated in the article. Reuse of AIP content is subject to the terms at: http://scitation.aip.org/termsconditions. Downloaded to IP: 130.102.42.98 On: Sun, 23 Nov 2014 05:02:50

temperature dependence between 300 and 1 K. Since they demonstrate weak inverse temperature dependence it does suggest mild increase in relaxation through the increase in lifetime of the OH–Ar complex as collision energy drops. The OH $A\,^2\Sigma-$Ar interaction potential at close range has been well determined and is sufficiently shallow as to not support vibrational quanta above 0 in the OH stretch.[30] The very strong inverse temperature dependence observed in vibrational relaxation is certainly consistent with a complex vibrational predissociation mechanism.

ACKNOWLEDGMENTS

Acknowledgment is made for the generous support of this work by the National Science Foundation under Grant No. CHE-9709656. We would also like to acknowledge useful discussions with Dr. David Crosley, Dr. Jorge Luque, Dr. Kristen Steffens, and Dr. Michael Heaven and we thank Dr. Michael Barfield for calculating the polarizability of the OH $A\,^2\Sigma$ state.

APPENDIX

The processes of relevance to the determination of OH $A\,^2\Sigma(v,N)$ relaxation rate coefficients are the following: The relaxation event itself

$$\mathrm{OH}\ ^2\Sigma(v,N)+\mathrm{Ar}\overset{k_{\mathrm{rel}}}{\rightarrow}\mathrm{OH}\ ^2\Sigma(v',N')+\mathrm{Ar} \tag{A1}$$

is in competition with several other processes, most importantly, fluorescence of the initial state

$$\mathrm{OH}\ ^2\Sigma(v,N)\overset{k_{fi}}{\rightarrow}\mathrm{OH}\ ^2\Pi_J(v'',N'') \tag{A2}$$

electronic quenching

$$\mathrm{OH}\ ^2\Sigma(v,N)+\mathrm{Ar}\overset{k_Q}{\rightarrow}\mathrm{OH}\ ^2\Pi(v',N')+\mathrm{Ar}, \tag{A3}$$

and possible predissociation

$$\mathrm{OH}\ ^2\Sigma(v,N)\overset{k_{pd}}{\rightarrow}\mathrm{O}+\mathrm{H}. \tag{A4}$$

The product of the relaxation in Eq. (A1) has two major subsequent pathways open to it that are of significance, mainly fluorescence

$$\mathrm{OH}\ ^2\Sigma(v',N')\overset{k_{fr}}{\rightarrow}\mathrm{OH}\ ^2\Pi_J(v'',N'') \tag{A5}$$

or subsequent quenching

$$\mathrm{OH}\ ^2\Sigma(v',N')+\mathrm{Ar}\overset{k'_Q}{\rightarrow}\mathrm{OH}(v'',N'')+\mathrm{Ar}, \tag{A6}$$

where the product of Eq. (A6) could be either the $A\,^2\Sigma$ or $X\,^2\Pi$ state. When the result of process (A6) yields OH in the $A\,^2\Sigma$ state subsequent fluorescence is detected and attributed to the relaxation event in Eq. (A1). In this way all product population for process (A1) with the sole exception of electronic quenching is accounted for.

Taking into consideration the local conditions in the free jet,[16] we can write a differential rate law for both the initially prepared reactant, OH $A\,^2\Sigma(v,N)$ of Eq. (A1), labeled *i*, or for the transfer state, tr, which is the product OH $A\,^2\Sigma(v',N')$ state of the relaxation Eq. (A1),

$$\frac{di}{dt}=-\left((k_{\mathrm{rel}}+k_Q)M_0\left(\frac{z_0}{z}\right)^2+k_{pd}+k_{fi}\right)i, \tag{A7}$$

$$\frac{dtr}{dt}=k_{\mathrm{rel}}M_0\left(\frac{z_0}{z}\right)^2 i-\left(k_{ftr}+k'_QM_0\left(\frac{z_0}{z}\right)^2\right)tr. \tag{A8}$$

The term M_0 describes the Ar stagnation density and z_0 is a nozzle diameter scaling factor.[16] These differential rate laws ignore the normal transport terms appropriate to kinetics in free jets since all of the rate processes studied in this paper occur over times comparable to fluorescent lifetimes. In these short times, jet transport is negligible and can be ignored. In other words, the initially prepared OH $A\,^2\Sigma$ excited state does not significantly move spatially during the kinetic study. Integration of Eq. (A7) yields

$$i(z,t)=i(z,t=0)\times\exp\left[-\left((k_{\mathrm{rel}}+k_Q)M_0\left(\frac{z_0}{z}\right)^2+k_{pd}+k_{fi}\right)t\right]. \tag{A9}$$

The integrated fluorescence of the initially prepared state at some position, *z*, in the jet is given by

$$I_i(z)=\int_0^\infty k_{fi}i(z,t)dt=\frac{k_{fi}i(z,t=0)}{(k_{\mathrm{rel}}+k_Q)M_0\left(\frac{z_0}{z}\right)^2+k_{pd}+k_{fi}}. \tag{A10}$$

Insertion of Eq. (A9) into (A8) followed by integration yields

$$\mathrm{tr}(z,t)=\frac{k_{\mathrm{rel}}M_0\left(\frac{z_0}{z}\right)^2 i(z,t=0)}{k'_{fr}-\left((k_{\mathrm{rel}}+k_Q)M_0\left(\frac{z_0}{z}\right)^2+k_{pd}+k_{fi}\right)}\times\left(\exp\left[-\left((k_{\mathrm{rel}}+k_Q)M_0\left(\frac{z_0}{z}\right)^2+k_{pd}+k_{fi}\right)t\right]-\exp[-k'_{fr}t]\right), \tag{A11}$$

where

$$k'_{ftr}=k_{ftr}+M_0\left(\frac{z_0}{z}\right)^2 k'_Q. \tag{A12}$$

The integrated fluorescence intensity from the transfer state, tr, is given by

$$I_{\mathrm{tr}}=\frac{k_{ftr}}{k'_{ftr}}\times\frac{k_{\mathrm{rel}}M_0\left(\frac{z_0}{z}\right)^2 i(z,t=0)}{\left((k_{\mathrm{rel}}+k_Q)M_0\left(\frac{z_0}{z}\right)^2+k_{pd}+k_{fi}\right)}. \tag{A13}$$

The ratio of the integrated intensities from the states, *i* and tr, yields

$$\frac{I_i}{I_{\mathrm{tr}}}=\frac{k_{fi}z^2}{k_{\mathrm{rel}}M_0z_0^2}+\frac{k'_Qk_{fi}}{k_{\mathrm{rel}}k_{fr}}. \tag{A14}$$

This article is copyrighted as indicated in the article. Reuse of AIP content is subject to the terms at: http://scitation.aip.org/termsconditions. Downloaded to IP: 130.102.42.98 On: Sun, 23 Nov 2014 05:02:50

Equation (A14) is equivalent to Eq. 6 in the text for $N - N'$ pure rotational state transfer.

For vibrational energy transfer, where the effects of v dependent predissociation or electronic quenching could become significant between the initial and transfer states, we chose an alternative method to determine the rate coefficient, k_{rel}. We still use Eq. (A13) to describe the fluorescence intensity of the vibrationally relaxed level. However, for comparison, we reference this intensity to that obtained when the same relaxed v' state, tr, is directly prepared by the laser. This laser prepared v' population will be called tr′. In this case, the initially prepared state population in the lower reference v' state, $\mathrm{tr}'(z,t=0)$, is related to the total fluorescence observed after preparation by

$$I_{\mathrm{ref}}=\frac{k_{fr}}{k'_{fr}}\mathrm{tr}'(z,t=0). \tag{A15}$$

Taking the ratio of Eq. (A13) to Eq. (A15) yields

$$\frac{I_{\mathrm{ref}}}{t_{ftr}}=\frac{\mathrm{tr}'(z,t=0)}{i(z,t=0)}\times\frac{(k_{pd}+k_{fi})z^2}{M_0 z_0 k_{\mathrm{rel}}} + \left(\frac{(k_{\mathrm{rel}}+k_Q)\mathrm{tr}'(z,t=0)}{k_{\mathrm{rel}}i(z,t=0)}\right), \tag{A16}$$

which is identical to Eq. 10 in the text for initial vibrational level v and transfer level v'.

[1] D. B. Atkinson, V. I. Jaramillo, and M. A. Smith, J. Phys. Chem. A **101**, 3356 (1997).
[2] D. B. Atkinson and M. A. Smith, Rev. Sci. Instrum. **66**, 4434 (1995).
[3] D. B. Atkinson and M. A. Smith, J. Phys. Chem. **98**, 5797 (1994).
[4] S. R. Leone J. Phys. Chem. Ref. Data **11**, 953 (1982).
[5] A. Jorg, U. Meier, and K. Kohse-Hoinghaus, J. Chem. Phys. **93**, 6453 (1990).
[6] R. A. Copeland, M. L. Wise, and D. R. Crosley, J. Phys. Chem. **92**, 5710 (1988).
[7] K. J. Rensberger, J. B. Jefferies, and D. R. Crosley, J. Chem. Phys. **90**, 2174 (1989).
[8] I. W. M. Smith, J. Chem. Soc., Faraday Trans. 2 **81**, 1849 (1985).
[9] R. K. Lengel and D. R. Crosley, J. Chem. Phys. **68**, 5309 (1978).
[10] R. K. Lengel and D. R. Crosley, J. Chem. Phys. **67**, 2085 (1977).
[11] R. K. Lengel and D. R. Crosley, Chem. Phys. Lett. **32**, 261 (1975).
[12] K. J. Rensberger, J. B. Jefferies, and D. R. Crosley, J. Chem. Phys. **90**, 2174 (1989).
[13] G. A. Raiche, J. B. Jefferies, K. J. Rensberger, and D. R. Crosley, J. Chem. Phys. **92**, 7258 (1990).
[14] K. R. German, J. Chem. Phys. **64**, 4065 (1976).
[15] M. Hawley and M. A. Smith, J. Chem. Phys. **95**, 8662 (1991).
[16] M. A. Smith and M. Hawley, in *Advanced Gas Phase Ion Chemistry*, edited by N. G. Adams and L. M. Babcock (JAI, Greenwich, CT, 1992), Vol. 1, p. 167.
[17] J. Reader, C. J. Sansonetti, and J. M. Bridges, Appl. Opt. **35**, 78 (1996).
[18] K. L. Steffens, J. Luque, J. B. Jefferies, and D. R. Crosley, J. Chem. Phys. **106**, 6262 (1997).
[19] I. L. Chidsley and D. R. Crosley, J. Quant. Spectrosc. Radiat. Transf. **23**, 187 (1980).
[20] D. R. Crosley and R. K. Lengel, J. Quant. Spectrosc. Radiat. Transf. **15**, 579 (1975).
[21] G. H. Dieke and H. M. Crosswhite, J. Quant. Spectrosc. Radiat. Transf. **2**, 97 (1962).
[22] J. Brzozowski, P. Erman, and M. Lyyra, Phys. Scr. **17**, 507 (1978).
[23] J. Luque and D. R. Crosley, ''LIFBASE Database and Spectral Simulation Program (Version 1.1),'' SRI International Report No. MP 96-001, 1996.
[24] J. A. Coxon, Can. J. Phys. **58**, 933 (1980).
[25] D. R. Miller, in *Atomic and Molecular Beam Methods*, edited by G. Scoles (Oxford University Press, Oxford, 1988), p. 14.
[26] D. R. Latimer and M. A. Smith, J. Chem. Phys. **101**, 3852 (1994).
[27] M. A. Smith, in *Current Topics in Ion Chemistry and Physics*, edited by C. T. Ng, T. Baer, and I. Powis (Wiley, New York, 1993), Vol. 2, p. 183.
[28] M. A. Smith, Int. Rev. Phys. Chem. **17**, 35 (1998).
[29] J. O. Hirschfelder, C. F. Curtiss, and R. B. Bird, *Molecular Theory of Gases and Liquids* (Wiley, New York, 1954).
[30] M. I. Lester, R. A. Loomis, L. C. Giancarlo, C. Chakravarty, and D. C. Clary, J. Chem. Phys. **98**, 9320 (1993).
[31] A. Jorg, U. Meier, and K. Kohse-Hoinghaus, J. Chem. Phys. **93**, 6453 (1990).

This article is copyrighted as indicated in the article. Reuse of AIP content is subject to the terms at: http://scitation.aip.org/termsconditions. Downloaded to IP: 130.102.42.98 On: Sun, 23 Nov 2014 05:02:50